Segregation and interdiffusion in (Fe,Co)/Pt superlattices

M. Björck,[1,*] G. Andersson,[1,†] B. Sanyal,[1] M. Hedlund,[1] and A. Wildes[2]
[1]*Department of Physics and Materials Science, Uppsala University, Box 530, SE-751 21 Uppsala, Sweden*
[2]*Institut Laue-Langevin, BP 156, 38042 Grenoble Cedex 9, France*

(Received 11 December 2007; revised manuscript received 19 December 2008; published 26 February 2009)

We report on the chemical structure of (Fe,Co)/Pt superlattices, which recently have shown high uniaxial magnetocrystalline anisotropy combined with high saturation magnetic moments. In particular, the homogeneity of the (Fe,Co) alloy is studied with a combination of x-ray and neutron reflectometry—the latter in a configuration where magnetic scattering is negligible. It is deduced, with support from off-specular x-ray reflectivity patterns and corresponding simulations, that the lower (Fe,Co)-on-Pt interface contains more Co than the upper Pt-on-(Fe,Co) interface. This can occur as Co interdiffuses into Pt more easily than Fe, as shown by density-functional calculations. The effect of this interdiffusion and segregation on the uniaxial anisotropy is discussed, and it is found that the previously observed discrepancy between experimental and theoretical anisotropy values can be quantitatively accounted for.

DOI: 10.1103/PhysRevB.79.085428 PACS number(s): 68.35.Ct, 68.35.Fx, 75.50.Bb

I. INTRODUCTION

During the last decades the study of thin films and other nanostructured materials has yielded considerable progress in our understanding of physical properties such as magnetoresistance and magnetocrystalline anisotropy. Recently, Burkert *et al.*[1,2] suggested a route, based on theoretical calculations, for obtaining a material with extremely promising recording media properties. The proposed material consisted of an originally body-centered-cubic (Fe,Co) alloy with about 60 at. % Co, which was tetragonally distorted until the c/a ratio was approximately 1.22, i.e., it attained a body-centered-tetragonal (bct) structure. In view of these calculations we have, in a previous study, synthesized (Fe,Co)/Pt superlattices which were found to be very close to the predicted optimum in terms of composition and c/a ratio.[3,4] However, the maximum uniaxial magnetocrystalline anisotropy energy, 208 μeV/atom, was only approximately one quarter of the predicted maximum value of 700–800 μeV/atom. The latter value of the uniaxial anisotropy constant is 50% larger than the leading FePt alloys, and at the same time the alloy is predicted to also have 50% larger magnetization, which is important for reducing the write field in hard drives.[2]

The superlattice structure by itself does not need to produce a material with optimal parameters, and therefore the value of 208 μeV/atom for a sample with bilayers of 3 monolayers (MLs) of (Fe,Co) alloy and 7 ML of Pt, repeated 23 times, was compared with density-functional theory (DFT) calculations on an equivalent structure.[3] The calculations gave a value of 380 μeV/atom, which was still almost twice as large as the measured value.

More detailed studies revealed that these structures showed a strong change in anisotropy with varying c/a ratio.[5] Another study, by Winkelmann *et al.*,[6] showed an out-of-plane easy axis for (Fe,Co) alloys of certain compositions deposited on Pd (001). They only estimated a lower bound on the magnetic anisotropy, giving less than 20% of the theoretically predicted value. In our case, one possible cause of the observed lowering of the magnetocrystalline anisotropy is interdiffusion, i.e., chemical mixing, between the (Fe,Co) and Pt layers as has been seen in the Co/Pt system.[7–9] The main aim of the present study is to investigate this, as well as the presence and influence of any segregation in the alloy layers.

These considerations are not isolated to this system alone, as it has become ever more obvious that the various defects arising at interfaces are extremely influential.[10] For almost all layered materials the sharpness of the interfaces is a key parameter for the degree of perfection in their functionality.[7–10] A further subdivision of the interface sharpness is the distinction between interdiffusion (chemical mixing) and roughness (steps or terraces) in these structures. Since these two contributions usually have different effects on the physical properties,[11,12] the ability to characterize the interdiffusion and the roughness independently is highly important. This is particularly the case for materials that are candidates for magnetic recording media such as the (Fe,Co)/Pt superlattices.

Measuring the extent of interdiffusion is far from a trivial task, and the simultaneous inclusion of both Fe and Co in the present materials further complicates the scenario. In some previous investigations, techniques such as medium-ion scattering (MEIS) on Co overlayers combined with annealing,[8] comparison to theoretical calculations,[9] and local probes, e.g., extended x-ray absorption fine structure (EXAFS),[7] have been used. Methods such as EXAFS and MEIS will have little or no contrast between Fe and Co due to their similarities in atomic weight and number of electrons. Also, local probes, such as EXAFS, are not spatially resolved. Transmission electron microscopy (TEM) which in principle could be useful for investigating the interfaces and segregation will also suffer from the lack of contrast between Fe and Co. In our first study of the (Fe,Co)/Pt structures[4] a number of TEM and electron-diffraction measurements were performed but could not resolve the composition within the (Fe,Co) or Pt layers nor the details at the interfaces. Neutron scattering techniques, on the other hand, have excellent contrast between Fe and Co.[13] Combining neutron and x-ray reflectivity will actually give elemental sensitivity, as well as a composition profile which is spatially resolved along the

scattering vector, due to the contrast variation between the different probes.

The neutron reflectivity measurements to be presented here were conducted with a strong magnetic field applied perpendicular to the surface, i.e., parallel to the scattering vector, to remove the magnetic contrast. It is a successful suppression of magnetic reflectivity in multilayer structures, rarely used in the past.[14] Due to the possible interdiffusion and segregation the analysis of the specular reflectivity was done with the so-called slicing technique.[15] The underlying physical principles of the composition profile were then analyzed with the aid of density-functional theory calculations of the surface segregation energies.

Diffuse reflectivity also has, in principle, the possibility to separate interdiffusion from roughness.[16] However, the only case known to the authors where this has been used is Ref. 17. In our present study, we analyzed diffuse x-ray reflectivity to extract quantitative widths of the interdiffused regions, and this information was then related back to the anisotropy.

In summary, the main aim of this paper is to provide a systematic investigation of the (Fe,Co)/Pt composition profile, and thereby to gain deeper understanding of the physical background of the magnetocrystalline anisotropy properties of this system. The route to the analysis of complex multilayer systems with respect to the elemental interdiffusion of the layers, especially using scattering techniques, should be applicable to a wide range of material combinations. Section II will briefly describe the sample preparation and the experimental equipment used. After that follows a detailed discussion including modeling of both reflectivities and anisotropy energies. It is concluded that the difference between observed and predicted anisotropy energies can be fully accounted for by a nonhomogeneous Co distribution in the (Fe,Co) layers, combined with interdiffusion at the interfaces.

II. EXPERIMENTAL DETAILS

The (Fe,Co)/Pt superlattices were grown on MgO (001) substrates with UHV-based magnetron sputtering from targets consisting of elemental Fe, Co, and Pt. Details of the growth conditions, including substrate treatment and buffer layer deposition (5.7 Å Fe and 39 Å Pt), can be found elsewhere.[4] The two samples intended for neutron measurements had the nominal thicknesses of 25 Å (Fe,Co) alloy and 35 Å of Pt. The sample denoted by FCP1 had a nominal Co concentration of 64 at. % and the sample denoted by FCP2 had a nominal composition of 40 at. % Co. Both samples were grown with 40 bilayer repetitions. The sample grown for off-specular reflectivity, denoted by FCP3, had the nominal thicknesses of 14.4 Å (Fe,Co) alloy and 19.6 Å Pt, repeated 20 times, with nominally 40 at. % Co.

The x-ray reflectivity measurements of samples FCP1 and FCP2 were conducted on a Bruker D8 with Cu $K\alpha$ radiation monochromatized using a two-bounce Ge monochromator. The secondary optics used was a slit in front of the detector. Sample FCP3 was measured on a Siemens D5000 with a graphite monochromator as secondary optics. This yielded lower background and higher intensity, making it more suitable for the off-specular measurements.

The neutron reflectivity experiments were conducted on instrument D17 at Institut Laue-Langevin, Grenoble. The measurements were collected in time-of-flight (TOF) mode with an unpolarized beam. In order to suppress the magnetic contrast from the samples, a 7 T superconducting magnet with a field perpendicular to the sample surface was installed. For each sample measurements at two different fields, 0.5 and 3 T, were conducted to verify that the sample magnetization was completely aligned with the field direction.

The Co concentration in the (Fe,Co) alloy was determined for a thicker (Fe,Co) film grown using the same deposition parameters as for the superlattice FCP1. X-ray photoelectron spectroscopy (XPS) measurements were performed on a Scienta ESCA-300 spectrometer using monochromated Al $K\alpha$ radiation (1486.7 eV). The measurements were done over the peaks corresponding to Fe $3p$, Co $3p$, and Pt $4f$. The electron take-off angle was 90° and the energy resolution of the electron analyzer was set to 0.4 eV.

III. RESULTS AND DISCUSSION

A. Neutron and x-ray reflectivity

The focus of this section will be on the neutron reflectivity results partly because of the special arrangement in the data collection. The x-ray reflectivity results will be presented later, together with composition profile simulations, in Sec. III B.

The unnormalized TOF data for sample FCP1 are shown in Fig. 1 for two different perpendicular fields, 0.5 and 3 T. In TOF mode, the specular scattering is expected to be at constant 2θ; in this case $2\theta=1.8°$. The data measured in 0.5 T have a clear Zeeman splitting, corresponding to neutron spin-flip scattering from components of magnetization that are in the plane of the sample. The theoretical positions of the resulting wings[14] are marked by lines. In a field of 3 T the Zeeman wings have disappeared almost completely. Only a very small signal, several orders of magnitude less intense than the specular reflection, can be seen. This verifies that the magnetization is aligned with the scattering vector at 3 T, and consequently the scattering under these conditions will be purely nuclear. The same behavior, although not shown here, was seen for sample FCP2.

Additional streaks of intensity can be seen in the 0.5 T data in Fig. 1. These features are Yoneda[18] wings; the positions of which are given by the condition that the exit or incidence angle is the same as the critical angle, θ_c. It should be noted that this Yoneda scattering is purely magnetic since it is not visible in the 3 T data.

The remaining part of the paper will focus on the refinement of the 3 T data since our interest is in the chemical structure of the samples. The data were normalized to direct beam measurements and the detector response was normalized using measurements from water. No appreciable off-specular scattering could be seen in the 3 T data.

The specular neutron reflectivity data from sample FCP1 will be presented together with simulations in Sec. III B. The corresponding data for sample FCP2 only showed one Bragg peak due to the lowering of contrast with increasing Fe con-

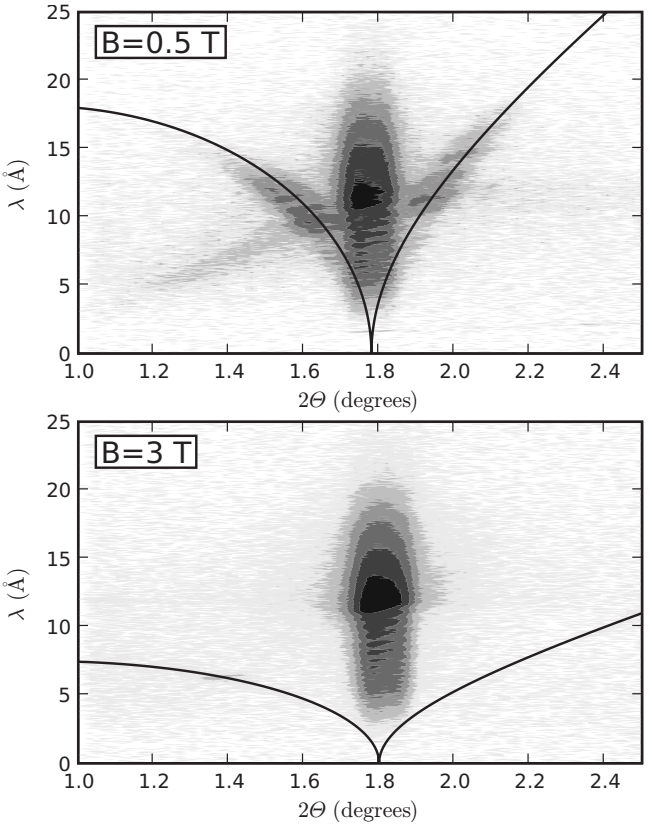

FIG. 1. Unnormalized TOF data for sample FCP1 at fields of 0.5 (upper) and 3 T (lower) plotted with a logarithmic intensity scale. The black lines show the theoretical positions of the Zeeman wings due to spin-flip scattering from components of the magnetization in the plane (Ref. 14). Note that the Zeeman wings have disappeared in the bottom panel. The additional streaks of intensity at 0.5 T are Yoneda wings.

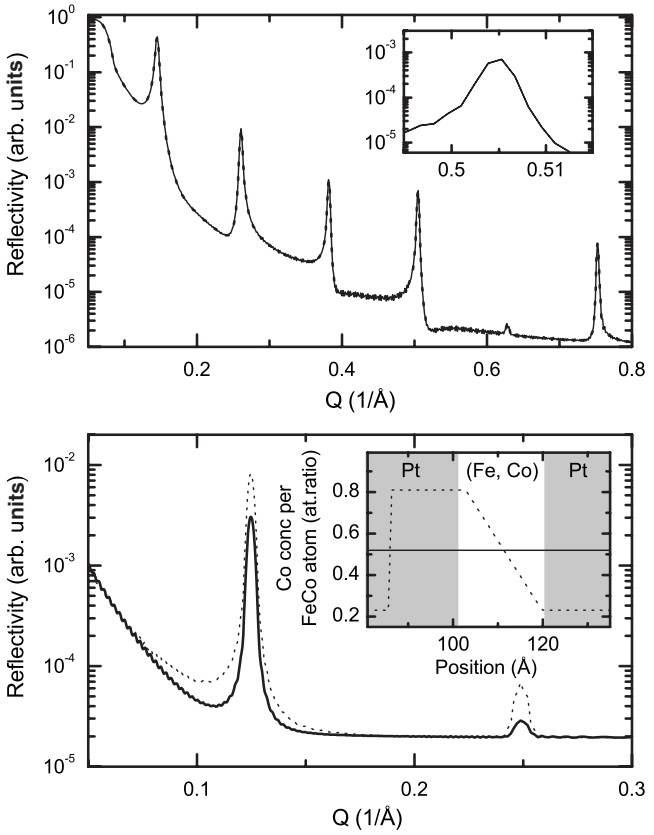

FIG. 2. Figure comparing the sensitivity to changes in the (Fe,Co) layer composition of x-ray reflectivity (top) and neutron reflectivity (bottom). The inset in the bottom panel shows the Co concentration per FeCo atom, cf. Fig. 6. Dotted lines represent an inhomogeneous (Fe,Co) layer and full lines represent a homogeneous (Fe,Co) layer both in the concentration plot and in the simulations.

centration in the alloy layers. This is a consequence of the individual neutron cross sections of Fe, Co, and Pt; the contrast between Fe and Pt is lower than between Co and Pt.[13] Consequently, only information about the average composition of that sample can be obtained, and the analysis is not presented here.

B. Composition profile

The x-ray data from sample FCP1, which will be shown later in Fig. 4, were first fitted with a standard model with Gaussian interface profiles using the so-called Nevot-Croce factors.[15] This fitting was never successful as the fits could not reproduce the fifth Bragg peak. Attempts to fit the x-ray data with a linear interface profile gave satisfactory results. However, upon including the neutron reflectivity data into the refinement process it became clear that a homogeneous (Fe, Co) layer in the sample model could not reproduce both data sets simultaneously. The difference in sensitivity between x-ray reflectivity and neutron reflectivity is exemplified in Fig. 2, where simulations are shown for one sample having (Fe, Co) layers with a Co composition gradient and one sample with (Fe, Co) layers without such a variation with depth of the Co content. The two simulated x-ray reflectivity curves show a perfect overlap, indicating a nonexisting sensitivity to any depth variation in Co concentration in the (Fe, Co) layer. The neutron reflectivity, on the other hand, shows a large separation between the simulations, highlighting the sensitivity of the method.

Thus, the developed models should contain the possibilities for homogeneous as well as segregated layers. In addition, since the composition could vary smoothly across the layers, the composition profiles used were continuous and later divided into thin slices, each about 0.8–0.9 Å thick. This made it possible to calculate the reflectivity according to the recursive algorithm of Parratt.[19] Due to the large increase in the number of layers, considering the 40 bilayer repetitions of the sample, the modeling was done using the single reflection approximation.[20] This approximation takes into account refraction and absorption but not multiple reflections. It is consequently a good approximation in all angular regions except close to the critical angle of total reflection.

The different models used for the composition profile are shown schematically in Fig. 3. We use two models in order to resolve model-independent features, since there is no guarantee that there is a unique solution for the element-specific composition profile. However, reproducible features

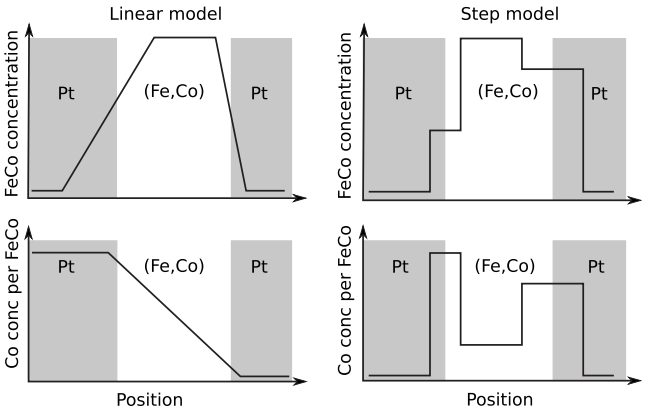

FIG. 3. The two different composition profile models used to refine the specular reflectivity data: the linear model (left) and the step model (right). The upper figures show the total (Fe,Co) content and the lower figures show the Co concentration per FeCo atom in the alloy layer. The gray regions show the location of the Pt layers in a perfect sample.

between the models can, to a large probability, be considered to be model independent and consequently not artifacts from the technique. The left parts of Fig. 3 show the *linear model* profile, which models all interfaces as having linear concentration gradients. Different linear gradients are used for the two interfaces, (Fe,Co) on Pt and Pt on (Fe,Co), respectively. In addition, the Co content within the (Fe,Co) layer is modeled with a linear profile where the mean value, height, and slope of the line are used as free parameters. The Co concentration per "FeCo" atom is defined as the relative amount of Co in the alloy, i.e., x in the formula unit $Fe_{1-x}Co_x$. The right parts of Fig. 3 show the *step model* where the (Fe,Co) layers are divided into three different sublayers, each of which has its separate thickness and amount of (Fe,Co) alloy. As shown in the lower-right panel, the Co content is also allowed to vary independently in the three sublayers. An additional smearing of the composition profile had to be included to get the model to fit to the data. The procedure used was a convolution of the composition profile with a Gaussian function, the width of which was also a free fitting parameter.

The two different models were implemented in the fitting environment *GenX*,[21] which uses the differential evolution method to refine multidimensional models to the data. The differential evolution method, being a genetic algorithm, is a global optimizer which efficiently avoids local minima, something that traditional algorithms often cannot achieve. In addition, *GenX* provides the possibility of defining continuous composition profiles (slicing), which is necessary in modeling layers consisting largely of interfaces.[15]

First the x-ray data were fitted using fixed Co concentration parameters. When a reasonable fit had been achieved the neutron data were added to the refinement process, and the procedure was repeated with the Co concentration parameters set free. It should be noted that changing the Co composition does not affect the x-ray data in any appreciable way. The results of the refinement process can be seen in Fig. 4 for the linear model (top) and the step model (bottom). As can also be seen in Fig. 4 the linear model quantitatively gives a slightly better fit than the step model.[22] In the following we will treat the two models as equally probable representations of the sample structure.

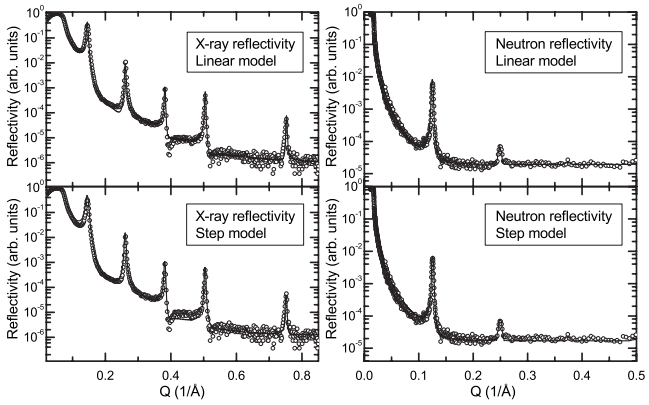

FIG. 4. The best fit (line) to the x-ray reflectivity (left) and neutron reflectivity (right) for the two models. The top graphs show the linear model and the lower graphs show the step model. The measured data are shown with circles.

The resulting elemental composition profiles from both models can be seen in Fig. 5. The profiles appear dissimilar, but it should be remembered that the real-space resolution of a reflectivity measurement, $d_{\min}$, is approximately equal to $2\pi/Q_{\max}$, where $Q_{\max}$ is the maximum scattering vector probed. Consequently, the resolution for the x-ray reflectivity is estimated to $d_{\min} \approx 8$ Å, which is about one third of the thickness of the (Fe,Co) layer. Thus, this explains why both models fit the measured data to a high extent. More importantly, Fig. 5 shows which features are model independent. The most prominent common feature is that the layers have

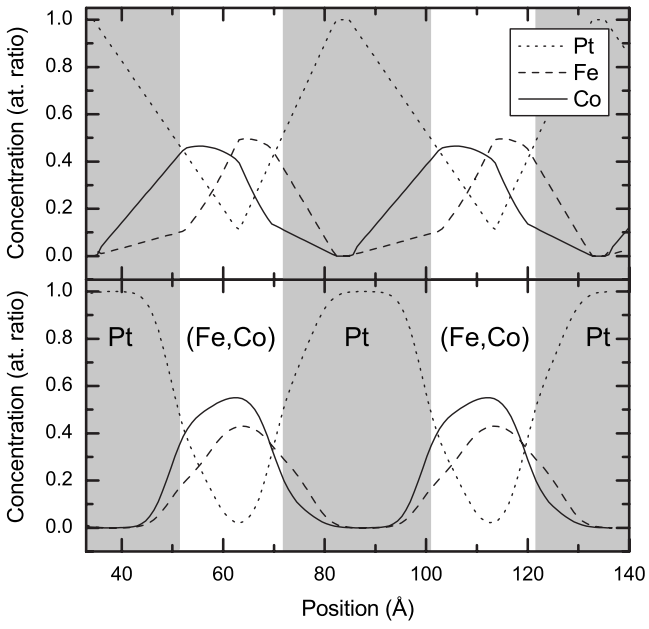

FIG. 5. The refined composition profiles for the linear model (upper) and the step model (lower). Dotted lines represent the Pt concentration, dashed lines the Fe concentration, and solid lines the Co concentration. The gray regions show the location of the Pt layers in a perfect sample. The position value is defined as increasing while moving upward through the layers from the substrate.

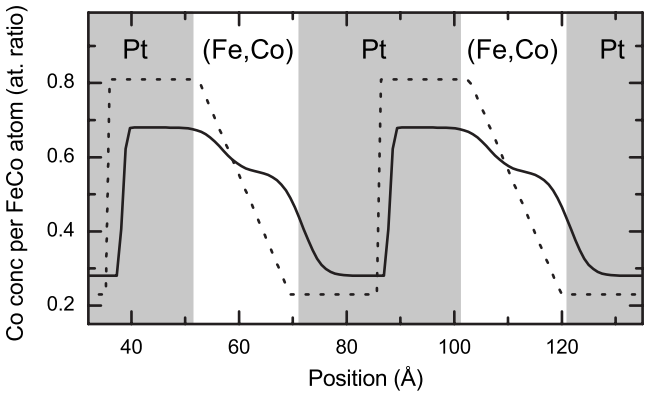

FIG. 6. The refined Co concentration per (Fe,Co) atom for the linear model (dashed) and the step model (solid). The gray regions show the location of the Pt layers in a perfect sample.

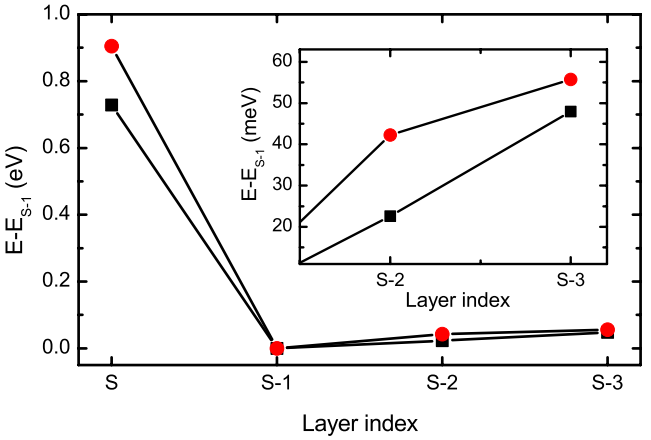

FIG. 7. (Color online) Total energies of 1 ML Fe (circles) and 1 ML Co (squares), respectively, on and inside a 10 ML Pt slab. Layer index S corresponds to the surface layer. The inset shows an enlargement for monolayers deeper inside the Pt slab.

an enhanced concentration of Co close to the (Fe,Co)-on-Pt interfaces and a corresponding enhancement of Fe content at the Pt-on-(Fe,Co) interfaces. This is also seen in Fig. 6 which displays the Co concentration per FeCo atom versus position along the growth direction. Since there are only two Bragg peaks in the neutron reflectivity data, it should also be noted that the only information available is the average composition and any asymmetry at the different interfaces. The extracted average composition of Co per $Fe_{1-x}Co_x$ unit (i.e., per FeCo atom) is $x=0.53(4)$ for the linear model and $x=0.56(4)$ for the step model, i.e., the models agree well with each other. They also agree very well with the value obtained from the XPS measurements, which was $x=0.53$.

C. Segregation and interdiffusion

One possible origin of the observed composition profile is that Fe and Co may segregate during the deposition process. However, the bulk phase diagram of the (Fe,Co) system shows no large mixing gaps at the deposition temperature.[23] Also, NMR studies of codeposited (Fe,Co) alloy film indicate no isolated Co regions in the films.[24,25] Another, more plausible, scenario is that Fe and Co atoms interdiffuse into the Pt upon deposition. If it is more favorable for Co than for Fe to diffuse into Pt, this can result in regions of enhanced Co and Fe concentrations in the composition profile.

In order to resolve any preference for interdiffusion for (Fe,Co) on Pt and Pt on (Fe,Co), respectively, theoretical calculations have been done with the plane-wave projector augmented wave method[26,27] within the density-functional theory and generalized gradient approximation as implemented in the Vienna *ab initio* simulation package (VASP). A 500 eV energy cutoff was used for the plane waves in the basis set. We have modeled the systems as slabs containing (a) 1 ML of Co and 10 ML of Pt, (b) 1 ML of Fe and 10 ML of Pt, (c) 1 ML of Pt and 12 ML of Fe, (d) 1 ML of Pt and 12 ML of Co, and (e) 1 ML of Pt and six bilayers of (Fe,Co). In all cases, the species containing 1 ML was kept at the surface and at different depths from the surface denoted in the following figures by S, S-1, etc., where S represents the surface layer. The atomic layers were relaxed in the (001) direction to obtain the equilibrium interplanar spacing. Figure 7, cases (a) and (b), shows the total energies of one Fe and Co layer on and inside the Pt slabs. In both cases, it is energetically favorable for the Fe (or Co) layer to stay in the subsurface layer. From the inset of Fig. 7 it is clear that it is comparatively easier for Co to diffuse in the bulk as the energy difference between S-1 and the deeper layers is lower than that of Fe. The results of the calculations with a Pt layer on and inside bcc Fe, Co, and (Fe,Co) slabs, cases (c)–(e), are presented in Fig. 8. One can see that contrary to the previous case, Pt prefers to stay on the surface of the three metallic slabs considered here. Thus, these results are in agreement with the observed trends from the refined models presented in Fig. 6. The greater affinity of Co to diffuse into the bulk of Pt causes an enrichment of Co at the lower interface and consequently less Co at the upper interface. If interdiffusion causes a significant broadening of the composition profile, the Pt-on-(Fe,Co) interface should be sharper than the (Fe,Co)-on-Pt interface. This is indeed the case that can be seen from the Pt composition profile for the linear model in the top graph of Fig. 5. It is not as clear for the step model, however, since upon inspection of the interface widths (i.e.,

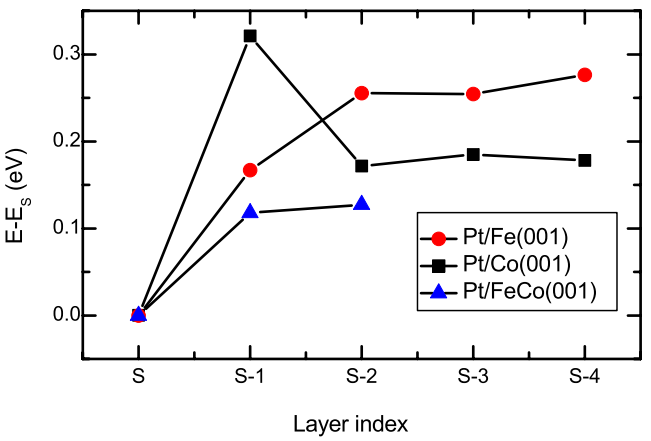

FIG. 8. (Color online) Calculated total energy of 1 ML Pt on and inside 12 ML slabs of Fe (circles), Co (squares), and (Fe,Co) (triangles). Layer index S corresponds to the surface layer.

the width of steps in the profile, cf. Fig. 3), the (Fe,Co)-on-Pt interface has a width of 8.1 Å whereas the Pt-on-(Fe,Co) interface has a width of 5.1 Å.

D. Implications for the anisotropy

To investigate the effect of interdiffusion on the anisotropy in Co/Pt multilayers, MacLaren and Victora[28,29] derived the following formula based on Néel's model.[30] Strictly speaking, application of Néel's model is not a reliable method for estimates of the magnetocrystalline anisotropy. However, when used with magnetocrystalline constants obtained for perfect systems, it was shown to give quantitative results.[28] The dependence of the interface anisotropy, K_i, on the amount of interdiffusion can thus be estimated by

$$2K_i = K_p \sum_{j=1}^{n} (P_j - P_{j+1})^2, \tag{1}$$

where K_p is the interface anisotropy of the perfect interface, P_j is the concentration of the magnetic material in layer j, and the summation runs over the n atomic layers in the superlattice period. For the studied superlattices a large strain contribution to the anisotropy has been found. The uniaxial anisotropy can be expressed as[5]

$$K_U = K_{\mathrm{VU}} + K_{\mathrm{strain}} + \frac{2K_i}{d_{(\mathrm{Fe,Co})}}, \tag{2}$$

where K_{VU} is the volume contribution, d_{FeCo} is the thickness of the (Fe,Co) layer, and K_{strain} is expressed as

$$K_{\mathrm{strain}} = K_{c/a}\left[(1-\sqrt{2})\left(\frac{c}{a}\right)^2 + \left(\frac{c}{a}\right) + \sqrt{2} - 2\right], \tag{3}$$

where $K_{c/a}$ is a constant describing the response of the anisotropy to the strain. The previously determined values[5] of the constants are $K_{c/a}=260$ MJ/m^3, $K_{\mathrm{VU}}=-3.16$ MJ/m^3, and $K_i=0.17$ mJ/m^2.

In order to experimentally measure the amount of interdiffusion between the layers so that its effect on the magnetocrystalline anisotropy could be estimated, off-specular reflectivity was recorded for sample FCP3 around the second and third Bragg peaks (Fig. 10). First, the specular reflectivity, shown in Fig. 9, was fitted using the *GenX* (Ref. 21) software with Nevot-Croce factors, i.e., ordinary Gaussian interface profiles. This was a more simplistic model than the one used to extract the composition profiles in Sec. III B. The specular fit, Fig. 9, was used to obtain total interface widths, including both roughness and interdiffusion, as well as the layer thicknesses. Then, the off-specular data were manually refined, allowing separation of roughness and interdiffusion contributions. The resulting simulations can be seen together with the measured off-specular reflectivity in Fig. 10. Values for the amount of interdiffusion at the two interfaces—a global jaggedness parameter[32] and in-plane as well as out-of-plane correlation lengths—are presented in Table I. The interdiffusion thickness corresponds to just above one monolayer of each constituent.

Using the amount of interdiffusion as measured from sample FCPN3, the anisotropy of a perfect interface can be estimated. However, for the layer thicknesses of the sample studied previously, 3 ML (Fe,Co) and 7 ML Pt,[3] the interface width is then comparable to the (Fe,Co) layer thickness. In order to include this in our calculations the composition profile for a sample with 3 ML (Fe,Co) has been simulated with the same amount of interdiffusion as sample FCP3. The resulting composition profiles, both continuous and subdivided

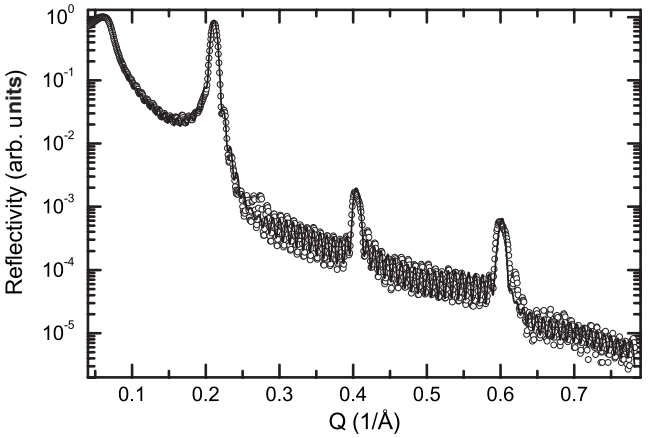

FIG. 9. Specular reflectivity from sample FCP3 (circles) and refined simulation (line) using Gaussian interface profiles (Nevot-Croce factors). The data were collected with Cu $K\alpha$ radiation.

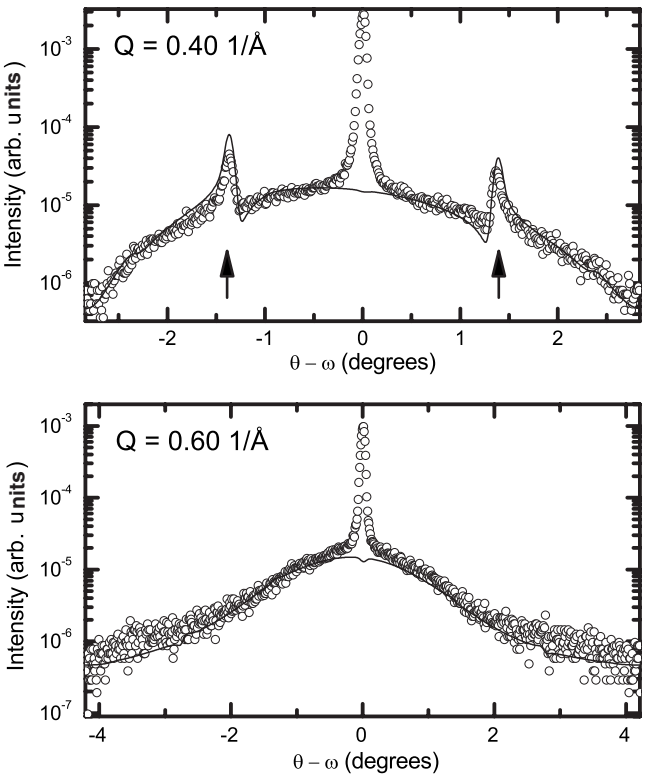

FIG. 10. Rocking curves around the second (upper) and third (lower) Bragg peaks of sample FCP3 measured with Cu $K\alpha$ radiation. Circles denote the measured data and lines denote the simulations. Note that the specular component, $\theta-\omega=0$, is not included in the simulations and that the panels have different scales. The arrows indicate the positions of resonant Bragg-type peaks which occur in vertically correlated multilayers (Ref. 31).

TABLE I. Refined values for sample FCP3. Only the parameters for the multilayer are presented. See text for details.

Parameter	Value
(Fe,Co) thickness	14.6 Å
Pt thickness	17.0 Å
(Fe,Co) roughness	2.9 Å
Pt roughness	2.3 Å
(Fe,Co) interdiffusion	1.9 Å
Pt interdiffusion	2.3 Å
In-plane correlation length	140 Å
Out-of-plane correlation length	100 Å
Jaggedness (Ref. 32)	0.8

into separate monolayers, are shown in Fig. 11.

From Eq. (1) the real interface contribution will be $2K_i = 0.28K_p$. This yields a total anisotropy for a perfect interface, as given by Eqs. (2) and (3), of $K_U = 4.19$ MJ/m^3 which should be compared to the value of $K_U = 2.16$ MJ/m^3 using the determined parameters. Thus, if interdiffusion can be avoided, e.g., by improving the deposition process in one or several ways, a large enhancement of the uniaxial anisotropy is expected. After including the uncertainties in the fit the anisotropy increase lies in the range of 30%–60 %. This enhancement can be compared to the theoretical calculations presented previously,[3] where the same 3 ML (Fe,Co)/7 ML Pt superlattice was modeled and which yielded a value 45% higher than the experimental results. The studies presented here indicate that a large part of the disagreement can be related to interdiffusion.

The segregation, as deduced from neutron reflectivity data, should also affect the anisotropy. However, it is reasonable to assume that the largest effect will be a shift of the observed maximum to higher Co concentrations in the (Fe,Co)/Pt as a whole, since the (Fe,Co) alloy will be depleted of Co and this has to be compensated.

IV. CONCLUSIONS

In conclusion, the homogeneity of the (Fe,Co) alloy layers in (Fe,Co)/Pt superlattices has been investigated by specular x-ray and neutron reflectometry. The results show that the (Fe,Co)-on-Pt interface contains more Co than the Pt-on-(Fe,Co) interface. Density-functional calculations show that Co diffuses more easily than Fe into Pt and that the other interface, Pt on (Fe,Co), is more stable. Thus, the observed composition gradient can originate from an interdiffused (Fe,Co)-on-Pt interface. The conclusions on interdiffused interfaces are also supported by simulations of the off-specular x-ray reflectivity data, where a large portion of the interface width appears to come from interdiffusion.

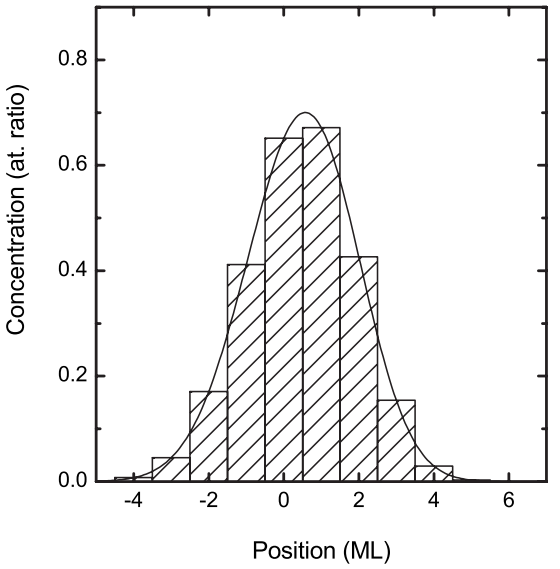

FIG. 11. The composition profile for 3 ML (Fe,Co) in Pt with the amount of interdiffusion from off-specular simulations. The line represents the continuous composition profile, whereas the bars correspond to the composition in each monolayer. The concentration is expressed as (Fe,Co)/Pt atomic ratio without distinction between Fe and Co atoms.

It is also shown that the disagreement previously seen between theoretical and experimental values of the uniaxial magnetocrystalline anisotropy energy can be accounted for quantitatively if interdiffusion is included in a simple model.[28] However, the influence of the composition gradient in the (Fe,Co) layers on the uniaxial anisotropy needs further study.

Lastly, this paper has shown that the tetragonally strained (Fe,Co) alloys still hold the possibility of obtaining a magnetocrystalline anisotropy energy comparable to or higher than, e.g., FePt alloys or Co/Pt multilayers, combined with twice the magnetic moment of the latter systems.[2] Possible routes to improvement would include a lowering of deposition temperature or dusting the interface with Fe atoms since deposition of Co on Fe produces a chemically sharp interface.[33]

ACKNOWLEDGMENTS

Financial support from the Swedish Research Council (VR), the Royal Physiographic Society in Lund, and the Göran Gustafsson Foundation is gratefully acknowledged.

*Present address: Paul Scherrer Institut, 5232 Villigen PSI, Switzerland.
†gabriella.andersson@fysik.uu.se

[1] T. Burkert, O. Eriksson, P. James, S. I. Simak, B. Johansson, and L. Nordstrom, Phys. Rev. B **69**, 104426 (2004).
[2] T. Burkert, L. Nordström, O. Eriksson, and O. Heinonen, Phys. Rev. Lett. **93**, 027203 (2004).
[3] G. Andersson, T. Burkert, P. Warnicke, M. Björck, B. Sanyal, C. Chacon, C. Zlotea, L. Nordström, P. Nordblad, and O. Eriksson, Phys. Rev. Lett. **96**, 037205 (2006).
[4] G. Andersson, M. Björck, H. Lidbaum, B. Sanyal, C. Chacon, C. Zlotea, and S. Valizadeh, J. Phys.: Condens. Matter **19**, 016008 (2007).
[5] P. Warnicke, G. Andersson, M. Björck, J. Ferré, and P. Nordblad, J. Phys.: Condens. Matter **19**, 226218 (2007).
[6] A. Winkelmann, M. Przybylski, F. Luo, Y. Shi, and J. Barthel, Phys. Rev. Lett. **96**, 257205 (2006).
[7] I. Chung, Y. Koo, and J. Lee, J. Appl. Phys. **87**, 4205 (2000).
[8] J. Kim, J. W. Lee, J. R. Jeong, S. C. Shin, Y. H. Ha, Y. Park, and D. W. Moon, Phys. Rev. B **65**, 104428 (2002).
[9] U. Pustogowa, J. Zabloudil, C. Uiberacker, C. Blaas, P. Weinberger, L. Szunyogh, and C. Sommers, Phys. Rev. B **60**, 414 (1999).
[10] M. Johnson, P. Bloemen, F. den Broeder, and J. de Vries, Rep. Prog. Phys. **59**, 1409 (1996).
[11] E. Holmström, L. Nordström, L. Bergqvist, B. Skubic, B. Hjörvarsson, I. Abrikosov, P. Svedlindh, and O. Eriksson, Proc. Natl. Acad. Sci. U.S.A. **101**, 4742 (2004).
[12] B. Skubic, E. Holmstrom, O. Eriksson, A. M. Blixt, G. Andersson, B. Hjorvarsson, and V. Stanciu, Phys. Rev. B **70**, 094421 (2004).
[13] V.-F. Sears, Neutron News **3**, 26 (1992); cross section table available at NIST web, http://www.ncnr.nist.gov/resources/n-lengths/
[14] G. Felcher, S. Adebwalla, V. De Haan, and A. Van Well, Nature (London) **377**, 409 (1995).
[15] M. Tolan, *X-ray Scattering from Soft-matter Thin Films* (Springer, New York, 1999).
[16] H. Zabel, Appl. Phys. A **58**, 159 (1994).
[17] M. Wormington, I. Pape, T. P. A. Hase, B. K. Tanner, and D. K. Bowen, Philos. Mag. Lett. **74**, 211 (1996).
[18] Y. Yoneda, Phys. Rev. **131**, 2010 (1963).
[19] L. Parratt, Phys. Rev. **95**, 359 (1954).
[20] V. Holy, U. Pietsch, and T. Baumbach, *High Resolution X-ray Scattering from Thin Films and Multilayers* (Springer, New York, 1999).
[21] M. Björck and G. Andersson, J. Appl. Crystallogr. **40**, 1174 (2007).
[22] The agreement between the model and the data [the figure of merit (FOM)] was measured by the mean-absolute error of the log transformed data, as defined in Ref. 34. Using this as the FOM in the refinement process led to an optimal FOM value for the linear model of 0.092, with 19 free parameters, while the step models had a FOM of 0.11, also with 19 free parameters. Thus, the linear model agrees better with the data.
[23] T. Nishizawa and K. Ishida, *Binary Phase Alloy Phase Diagrams*, 2nd ed. (ASM International, Materials Park, 1996).
[24] J. Jay, M. Wójcik, and P. Panissod, Z. Phys. B: Condens. Matter **101**, 471 (1996).
[25] M. Wójcik, J. Jay, P. Panissod, E. Jedryka, J. Dekoster, and G. Langouche, Z. Phys. B: Condens. Matter **103**, 5 (1997).
[26] G. Kresse and J. Hafner, Phys. Rev. B **47**, 558 (1993).
[27] G. Kresse and J. Furthmüller, Phys. Rev. B **54**, 11169 (1996).
[28] J. MacLaren and R. H. Victora, J. Appl. Phys. **76**, 6069 (1994).
[29] R. H. Victora and J. M. MacLaren, Phys. Rev. B **47**, 11583 (1993).
[30] M.-L. Néel, J. Phys. Radium **15**, 225 (1954).
[31] V. Holý and T. Baumbach, Phys. Rev. B **49**, 10668 (1994).
[32] J. P. Schlomka, M. Tolan, L. Schwalowsky, O. H. Seeck, J. Stettner, and W. Press, Phys. Rev. B **51**, 2311 (1995).
[33] J. Jay, E. Jêdryka, M. Mójcik, J. Dekoster, G. Langouche, and P. Panissod, Z. Phys. B: Condens. Matter **101**, 329 (1996).
[34] M. Wormington, C. Panaccione, K. M. Matney, and D. K. Bowen, Philos. Trans. R. Soc. London, Ser. A **357**, 2827 (1999).